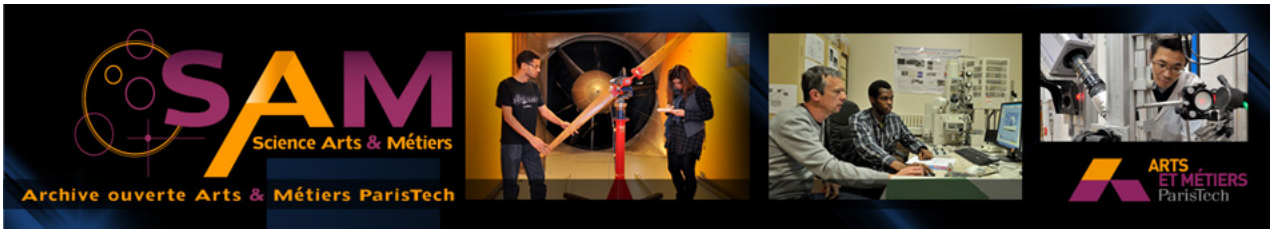

# Effect of Surface Roughness in the Determination of the Mechanical Properties of Material Using Nanoindentation Test

Yang Xia,[1] Maxence Bigerelle,[2] Julie Marteau,[1] Pierre-Emmanuel Mazeran,[1] Salima Bouvier,[1] and Alain Iost[3]

[1]Laboratoire Roberval de Mécanique, CNRS-UMR 7337, University of Technology of Compiègne, Compiègne, France
[2]Équipe Matériaux, Surfaces et Mise en forme, TEMPO, LAMIH, UMR 8201, Université de Valenciennes, Valenciennes, France
[3]Laboratoire de Mécanique de Lille, CNRS-UMR 8107, Arts et Métiers ParisTech, Lille, France

**Summary:** A quantitative model is proposed for the estimation of macro-hardness using nanoindentation tests. It decreases the effect of errors related to the non-reproducibility of the nanoindentation test on calculations of macro-hardness by taking into account the indentation size effect and the surface roughness. The most innovative feature of this model is the simultaneous statistical treatment of all the nanoindentation loading curves. The curve treatment mainly corrects errors in the zero depth determination by correlating their positions through the use of a relative reference. First, the experimental loading curves are described using the Bernhardt law. The fitted curves are then shifted, in order to simultaneously reduce the gaps between them that result from the scatter in the experimental curves. A set of shift depths, $\Delta h_c$, is therefore identified. The proposed approach is applied to a large set of TiAl6V4 titanium-based samples with different roughness levels, polished by eleven silicon carbide sandpapers from grit paper 80 to 4,000. The result reveals that the scatter degree of the indentation curves is higher when the surface is rougher. The standard deviation of the shift $\Delta h_c$ is linearly connected to the standard deviation of the surface roughness, if the roughness is high-pass filtered in the scale of the indenter (15 μm). Using the proposed method, the estimated macro-hardness for eleven studied TiAl6V4 samples is in the range of 3.5–4.1 GPa, with the smallest deviation around 0.01 GPa, which is more accurate than the one given by the Nanoindentation MTS$^{TM}$ system, which uses an average value (around 4.3 ± 0.5 GPa). Moreover, the calculated Young's modulus of the material is around 136 ± 20 GPa, which is similar to the modulus in literature.

**Key words:** roughness, hardness, indentation size effect, first contact, nanoindentation

## Introduction

The mechanical properties of solids largely determine the performance of devices. With the miniaturization of systems and the development of high-precision instruments, the characterization of mechanical properties at micro or nanometer scale has become a very active area (Mukhopadhyay and Paufler, 2006). Nanoindentation test is a common and convenient means to investigate the near-surface mechanical properties, at depths of a few micrometers (Oliver and Pharr, 2010). The hardness, a particularly interesting mechanical property of material, can be extracted from the experimental load–depth curves that are recorded during the indentation test (Oliver and Pharr, '92). In practice, the recording of load–depth data begins from the first contact between the indenter and the specimen surface. All the subsequent depth measurements will be relative to the first contact depth. Therefore, the accuracy of hardness is directly affected by the identification of this first contact point (Fischer-Cripps, 2000). Usually, it is set as the smallest obtainable force of the instrument or as a specific stiffness given by the user (Fischer-Cripps, 2006). However, it is still difficult to detect the initial contact point accurately, due to the existence of systematic errors and materials-related factors (Grau *et al*., '94; Ullner, 2000; Bigerelle *et al*., 2007b; Kalidindi and Pathak, 2008; Wei *et al*., 2008). Among all the materials-related factors, some degree of surface

Contract grant sponsor: China Scholarship Council (CSC); contract grant number: 2010008045.

Address for reprints: Yang Xia, Laboratoire Roberval de Mécanique Roberval, Centre de recherches de Royallieu, University of Technology of Compiègne, Rue Personne de Roberval, 60205 Compiègne, France
E-mail: yang.xia@utc.fr

roughness is almost inevitable in nanoindentation tests, which thus introduces inaccuracies of first contact detection. Hence, roughness is considered a crucial issue in understanding the indentation size effect (ISE), i.e. a significant increase in hardness with the decrease of depth (Ohmori *et al*., 2003; Zhang *et al*., 2004; Kim *et al*., 2007; Zhanga and Xu, 2002). It is worth noting that the literature overview mentions several reasons that may explain the ISE. For crystalline materials, some authors pointed out that the ISE can be explained by the occurrence of geometrically necessary dislocations (Gao and Huang, 2003), and they developed models based on strain gradient plasticity (Nix and Gao, '98) to describe this phenomenon. Others state that the ISE is related to surface energy (Zhang *et al*., 2004; Kim *et al*., 2007). Others interpret the ISE as the effect of extrinsic factors such as the blunt tip on a sharp indenter, an oxide layer, chemical contamination and the friction between the test specimen and the indenter (Liu and Ngan, 2001; Qu *et al*., 2004; Kim *et al*., 2005; Aguilar-Santillan, 2008). In this paper, the aim is to highlight the contribution of the surface roughness to the ISE occurrence. It is clear that the latter cannot be considered as a major effect. However, it still has an impact on ISE. The geometrically necessary dislocation contribution is among the most frequently reasons given to explain the ISE. However, this phenomenon still exists in non-crystalline materials (e.g. glass, Huang *et al*., 2010; Jang *et al*., 2011), which indicates that other reasons are behind the indentation size effect. The influence of surface roughness on ISE can be reduced with a sufficient surface preparation (e.g. polishing), but the latter would introduce some surface hardening, which would affect the hardness measurement at the early stage of indenter penetration. Therefore, surface roughness cannot be completely ignored when dealing with the ISE.

In the present work, a quantitative model for macro-hardness and indentation size effect measurements is proposed. This model can effectively decrease the errors on hardness values and reliably identify the indentation size effect resulting from an incorrect detection of the first contact between the indenter and the sample displaying a rough surface. The most significant feature of this model is the simultaneous statistical treatment for a large set of the nanoindentation loading curves $I$, whose locations are set by a specific definition of the first contact error $(\Delta h_{ci,i\in I})$, defined as a gap between the individual experimental loading curve $i$ and the simulated one using Bernhardt's law (Bernhardt, '41). The proposed approach is applied on nanoindentation data of eleven TiAl6V4 samples with variant levels of roughness. The latter are obtained by polishing the surface using grit papers from 80 to 4,000. The model is used in the estimation of the macro-hardness and the indentation size effect. The influence of surface roughness on the hardness evaluation is examined in order to identify the factors that affect the error in the contact detection. A multi-scale analysis of the roughness is carried out to determine the most appropriate scale for the evaluation of each roughness parameter. An original statistical method, based on the measured roughness data and on the first contact error, is proposed in order to identify the suitable scale.

## Materials and Methods

### Materials

The samples are cut from a cylinder of TiAl6V4 alloy having a diameter of 30 mm. Each sample is 20 mm height. The chemical composition (wt%) is Al (6.13), V (4.00), Fe (0.11), O (0.11), C (0.004), N (0.006), Y (<0.001), H (0.0007), and Ti (base).

### Polishing

A specific automatic polishing machine (Planopol-3 and Pedemax-2 from Struers$^{TM}$, Champigny sur Marne cedex, France) which has a dual off-center rotating movement is used in the experiments. Eleven different abrasive papers of silicon carbide grain are used. The grain sizes are from 200 to 5 μm. The corresponding grits are: 80, 120, 180, 220, 320, 500, 800, 1,000, 1,200, 2,400, and 4,000. Each grinding step is systematically performed with a new silicon carbide paper under a fixed load and time (150 N, 3 min) using water lubrication at 300 revolutions per minute. In the paper, the different specimens are labeled with the number of the final grit paper used to polish them.

### Roughness Measurement

The roughness of the abraded specimens is measured using a tridimensional (3D) roughness stylus profilometer (TENCORTM P10). Its vertical sensitivity is about 1 nm, and its horizontal sensitivity is about 50 nm. The 2 μm radius stylus tip is used under a 50 μN load. Due to polishing, a fractal aspect of the roughness emerges (Bigerelle *et al*., 2005, 2007a, 2008). The polished surface is considered as isotropic and 2D measurements are used to analyze the fractal aspect of the roughness (Bigerelle *et al*., 2002). An accurate analysis of the surface is performed using two-dimensional (2D) high-resolution profiles. Each profile is recorded on a length of 5 mm (25,000 points) at a speed 200 μm/s. For each sample, 30 profiles are randomly recorded, and a statistical treatment of the results is performed. The 3D surface measurement is made using an optical interferometer (Zygo NewView$^{TM}$ 7300, Darmstadt, Germany). Measurements are taken with a 50× Mirau objective to provide a 0.14 mm × 0.11 mm measurement area. The

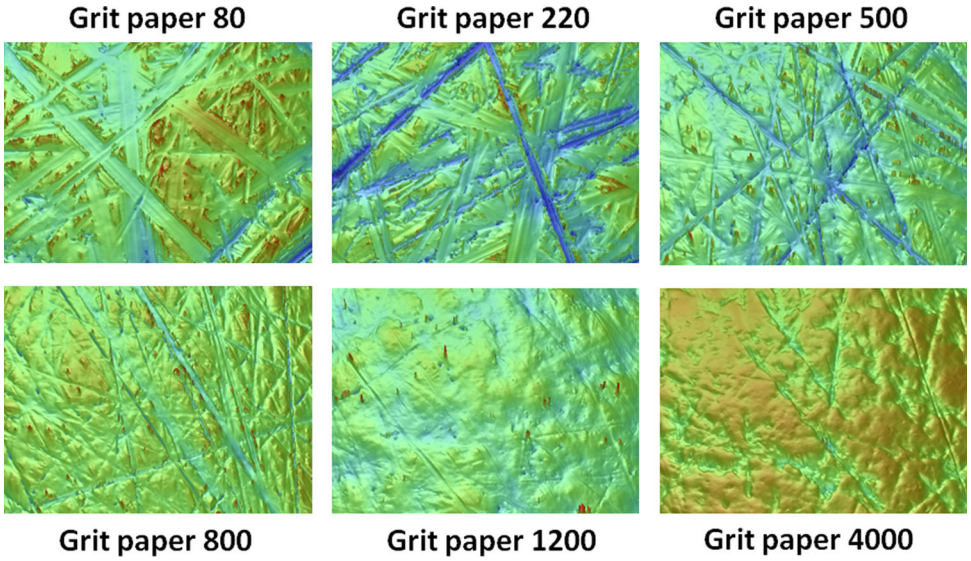


Fig 1. 3D topology of initial surfaces of TiAl6V4 samples with different roughness using optical interferometer.

optical resolution in lateral spatial ($x$–$y$ axis) and vertical spatial ($z$-axis) is 0.52 μm and 1 nm, respectively. Vertical scanning interferometry technique (Bipolar scan) was used to measure the surfaces. The maximum vertical scan length is 100 μm to assure all peaks and valleys of the surface can be measured. The scan time of one measurement is 7 s. Figure 1 shows the 3D topology surface of samples polished by grit papers 80, 220, 500, 800, 1,200, and 4,000. Here, deep valleys (dark colors) and high peaks (light colors), due to the grinding process, can be easily observed in the surface structure.

## Nanoindentation Tests

Nanoindentation tests are made with a Nano Indenter XP, using a Berkovich tip. The instrument is on an anti-vibration base and is located in an ambient temperature cabinet, which provides a thermally stable environment. Experiments are performed using the continuous measurement method (CSM) at a constant strain rate (0.05 $s^{-1}$) until the maximum indentation depth of 3,000 nm is achieved. One hundred indentations are made for each TiAl6V4 specimen. Figure 2 shows the loading curves versus indentation depth obtained for the specimen polished with grit paper 2,400. Only the loading parts of the curves are shown. To avoid any statistical artifacts, only the parts of the curves whose load value are less than 0.8 times the maximum load are kept.

## Pile-Up Volume Measurement

To quantify the effect of pile-up on hardness in the nanoindentation test, the indentation imprints are measured with optical interferometer. All the parameters for the interferometer are same with the initial 3D surface measurement. Then the volume of indentation ($V_{\text{indent}}$) and the volume of pile-up ($V_{\text{pileup}}$) around the indentation are estimated. The preprocessing of the surface profile is described below. It is well known that a typical engineering surface consists of a range of spatial frequencies. For this reason, a Gaussian filtering technique is used to separate the roughness from the waviness phenomena of the profile. Figure 3 shows (a) the source surface, (b) the filtered roughness surface, and (c) the filtered waviness surface of the specimen polished by grit paper 2,400. The global form around the indentation print is removed by taking a third-degree polynomial regression, without considering the indentation print into its computation. The result has been shown in Figure 3d.

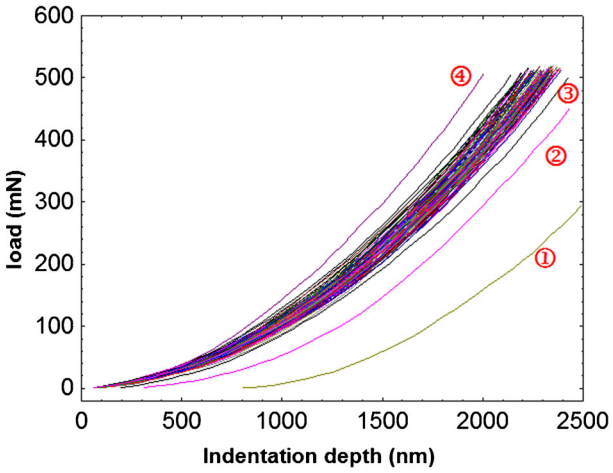


Fig 2. One hundred experimental loading–depth curves of the sample polished by grit paper 2,400.

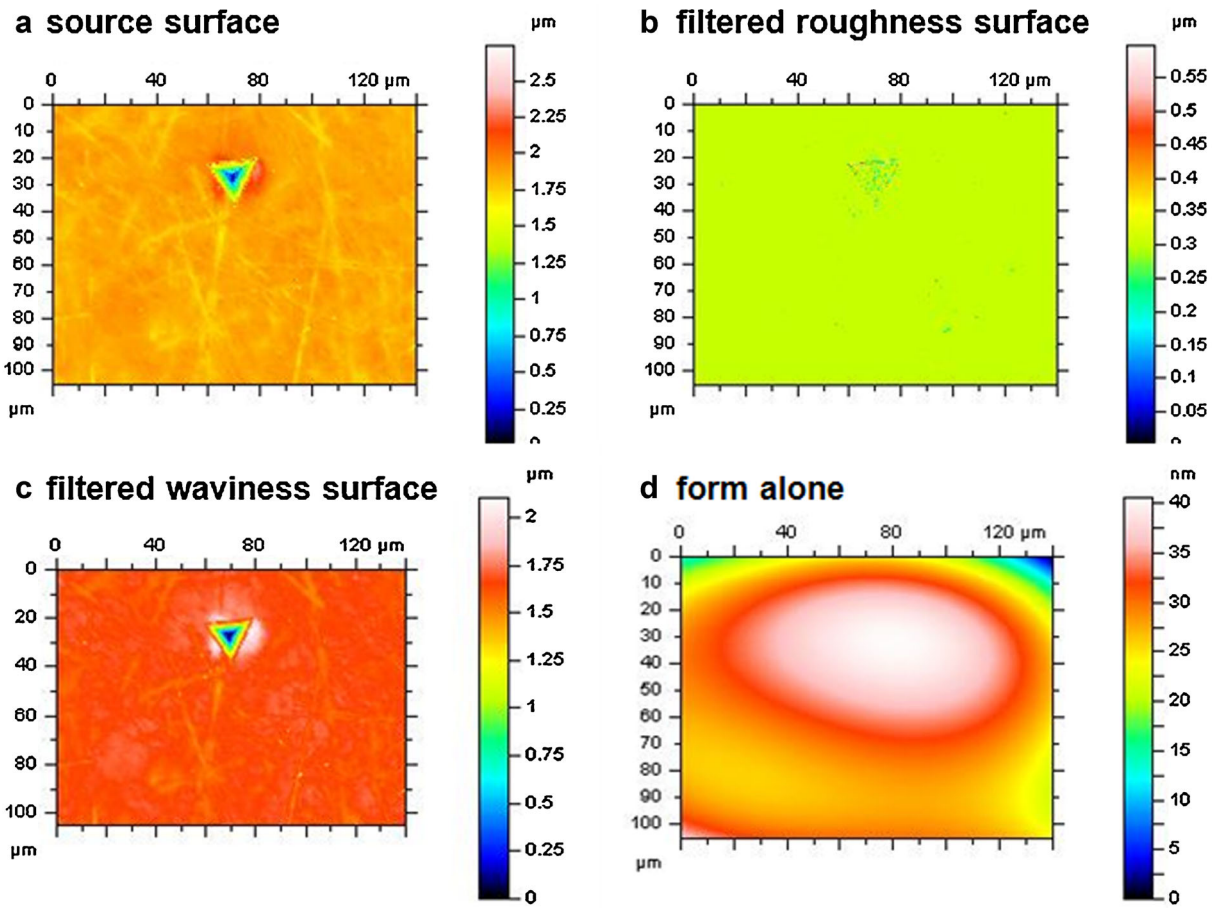


Fig 3. Images of (**a**) source surface, (**b**) filtered roughness surface, (**c**) filtered waviness surface, and (**d**) the form alone of the sample polished by grit paper 2,400.

The zoomed 3D image of one indentation of the specimen polished with grit paper 2,400 is shown in Figure 4. The volume of indentation and pile-up are measured. By measuring the pile-up on each side of the triangle formed by the indent, the total volume of the pile-up is estimated (see Fig. 5).

## Theory and Model

*Hardness treatment*

For geometrically similar indenters, a quadratic relationship between the load P and the indentation depth h is appropriate to describe the loading indentation curve. It is known as Kick's law (Kick, 1885):

$$P = Ch^2, \tag{1}$$

where $C$ is a parameter that depends on both the indenter shape and the material. The significance of this law is that the material hardness remains constant regardless of the applied force to the indenter. Unfortunately, Kick's law fails to describe the initial part of the indentation curves, which may be caused by the occurrence of the ISE. The Bernhardt's model (Bernhardt, '41) was proposed to correct Kick's formula by adding a linear term that considers the indentation size effect:

$$P = \alpha_1 h^2 + \alpha_2 h, \tag{2}$$

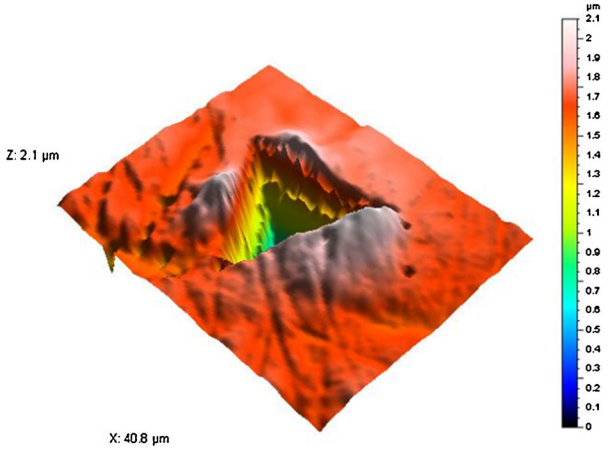


Fig 4. Zoomed 3D image of one indentation of the sample polished by grit paper 2,400.

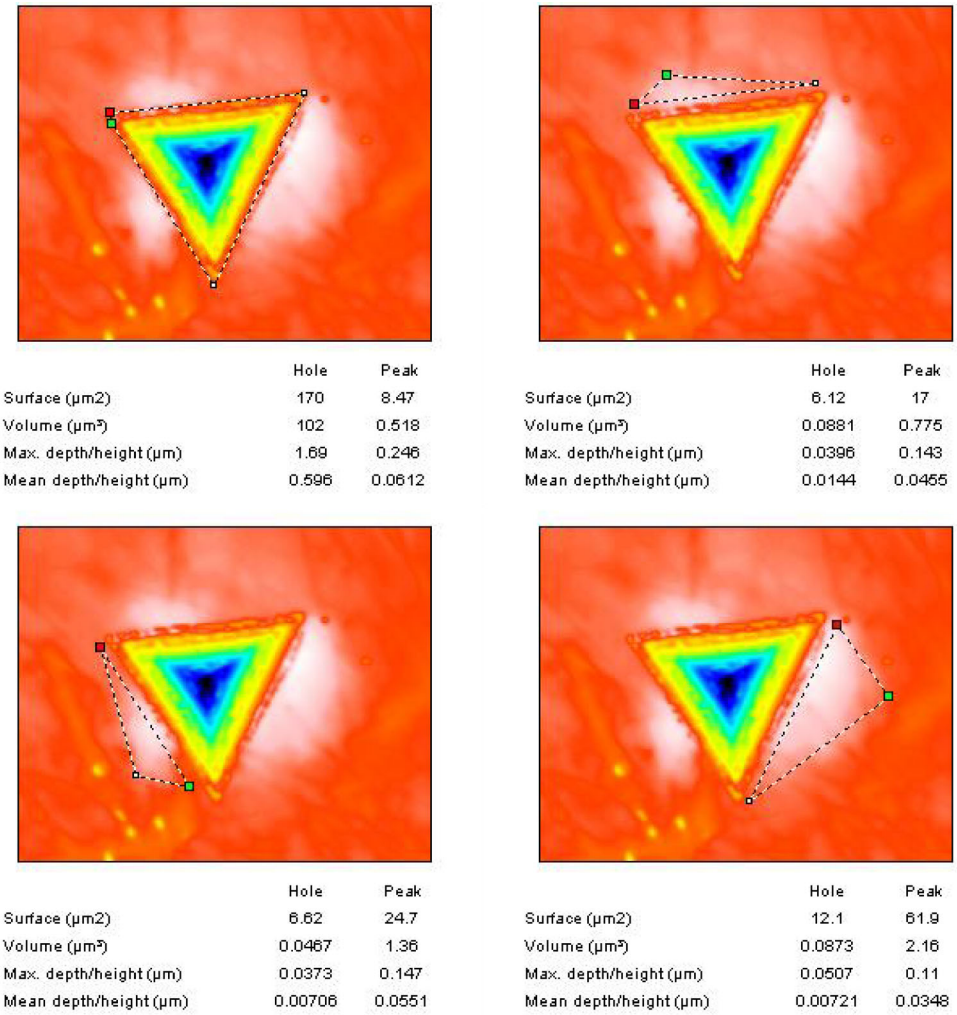


Fig 5. Diagram of the indentation volume ($V_{indent}$) and pile-up volume ($V_{pileup}$) of the sample polished by grit paper 2,400.

where $\alpha_1$ and $\alpha_2$ are parameters related to the geometry of the indenter tip and the material properties. The linear term $\alpha_2$ aims to characterize the load dependence with increasing indentation depth at the beginning of the *P–h* curve. Bernhardt's model can also be written using the contact depth $h_c$ defined by the Oliver and Pharr method:

$$h_c = h - \varepsilon \frac{P}{S}, \tag{3}$$

where $S$ is the stiffness of the contact and $\varepsilon$ is a geometrical constant equal to 0.75 for a Berkovich indenter. Therefore, Equation (2) could be rewritten as follows:

$$P = \alpha(H_0 h_c^2 + \beta h_c), \tag{4}$$

where $\alpha$ is constant that depends on the geometry of the indenter, $H_0$ is the macro-hardness of the specimen, and $\beta$ is the parameter related to the ISE (i.e. the linear part of the *P–h* curve). In order to take into account errors related to the detection of the first contact point, the contact depth $h_c$ in Equation (4) is replaced by $h_c + \Delta h_c$ where $\Delta h_c$ stands for the deviations that may exist between the original experimental curves and Equation (4). Hence, the latter is modified as follows:

$$P = \alpha[H_0(h_c + \Delta h_c)^2 + \beta(h_c + \Delta h_c)] \tag{5}$$

and yields to (after neglecting the term $\Delta h_c^2$):

$$P = \alpha[H_0 h_c^2 + (2H_0 \Delta h_c + \beta)h_c + H_0 \Delta h_c^2 + \beta \Delta h_c]. \tag{6}$$

When dealing with the reproducibility of the *P–h* curves in the nanoindentation test, most of the proposed methods treat the experimental curves separately, and then compute the material properties (e.g. hardness) by averaging the values given by the different data. The

method developed in this paper is different in the sense that all the experimental curves are considered at the same time, and then a single set of material properties is calculated. The macro-hardness $H_0$ and the ISE factor $\beta$ are obtained using a least square regression analysis, as indicated in Equation (7). In the same minimization procedure, the deviations $\Delta h_c$ are identified for the set of the experimental curves:

$$\min_{H_0,\Delta h_1,\ldots,\Delta h_n,\beta} \sum_{i=1}^{n}\sum_{j=1}^{p_j} \{P_{i,j} - \alpha[H_0 h_{cj}^2 + (2H_0\Delta h_{ci} + \beta)h_{cj} + H_0\Delta h_{ci}^2 + \beta\Delta h_{ci}]\}^2 \quad (7)$$

where $j$ refers to a point belonging to curve $i$.

The bootstrap is a statistical technique that has been used to compute several factors: constitutive laws with the punch test (Isselin *et al.*, 2006), fatigue life time prediction (Bigerelle and Iost, '99), the adhesion properties of materials (Bigerelle and Anselme, 2005), and roughness influence on materials properties (Najjar *et al.*, 2003). In order to determine the confidence intervals on $H_0$ and $\beta$, a double bootstrap over a hundred original experimental loading curves for each specimen is achieved. The first bootstrap is used to ensure that the observed data are independent and identically distributed. The second bootstrap achieves a simple random sampling with replacement, and is repeated 1,000 times in order to reproduce the specimen heterogeneity (Marteau *et al.*, 2013). Figure 6 shows the relations between the hardness, the indentation size effect factor, and the first contact errors after the bootstrap. The results clearly indicate that these three values are not correlated with each other, which means that the problem is well formulated from a statistical point of view (Isselin *et al.*, 2006). Hence, there is confidence that viable mechanical properties are selected.

Figure 7 shows the results for the specimen polished using grit paper 2,400. Very effective scatter reduction is obtained for the $P$–$h$ curves (see Fig. 2), which would yield to a more accurate macro-hardness estimation. The distribution of the first contact errors is given in Figure 8. The subpopulation gathering of a few curves, indicated by four red arrows, corresponds to the four experiment curves labeled by numbers in Figure 2. This is part of the systematic errors that result from a false detection of the

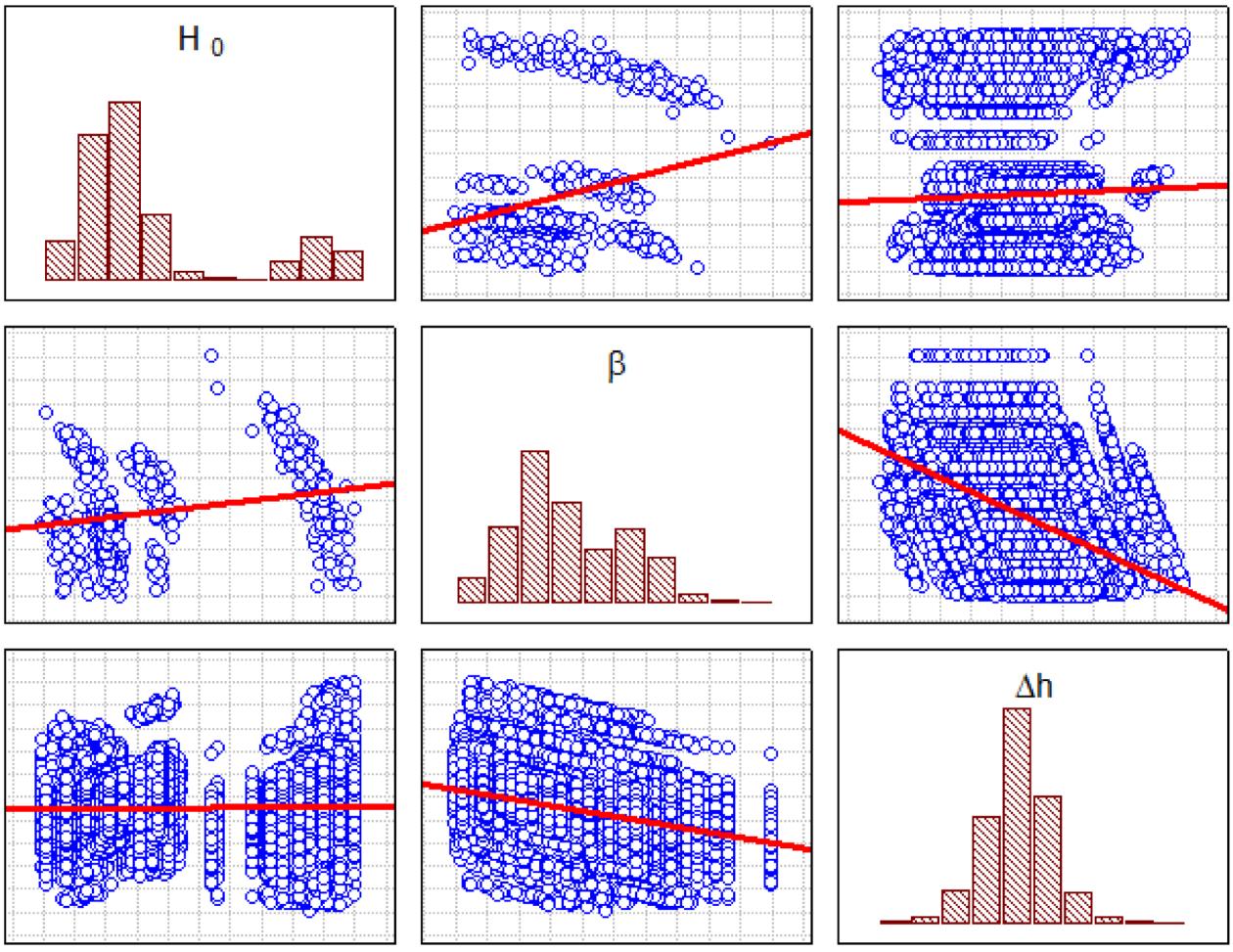


Fig 6. Relations among the hardness, indentation size effect, and first contact error after the bootstrap.

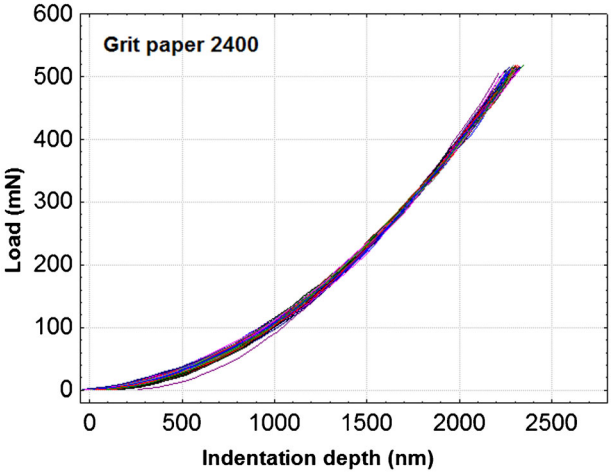


Fig 7. Shifting curves of 100 loading curves of the sample polished by grit paper 2,400 (see Fig. 2).

first contact by the nanoindentation device. On the other hand, the second subpopulation (including many curves) shows lower scatter, which may arise from different phenomena such as measurement noise, indenter tip defect, temperature variation, or roughness. All the mechanical properties are calculated using the data belonging to this part.

Figures 9 and 10 indicate the distributions of macro-hardness $H_0$ and the ISE factor $\beta$, respectively, for the specimen polished with the grit paper 2,400. The mean value of the macro-hardness is 3.645 GPa, and the deviation is 0.008 GPa. For the coefficient $\beta$, the mean value is 774 mN/nm, and the deviation is 113 mN/nm. The small deviation of the macro-hardness indicates that this quantitative method allows a reduction of the errors and provides a more reliable assessment of the material parameters.

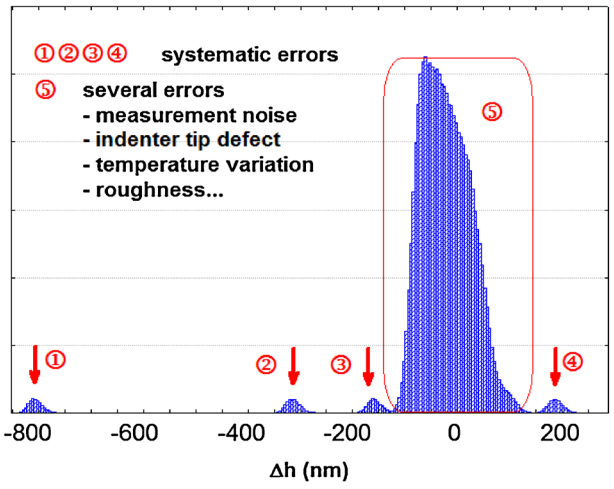


Fig 8. Statistical distribution of the first contact error $\Delta h_c$ of sample polished by grit paper 2,400.

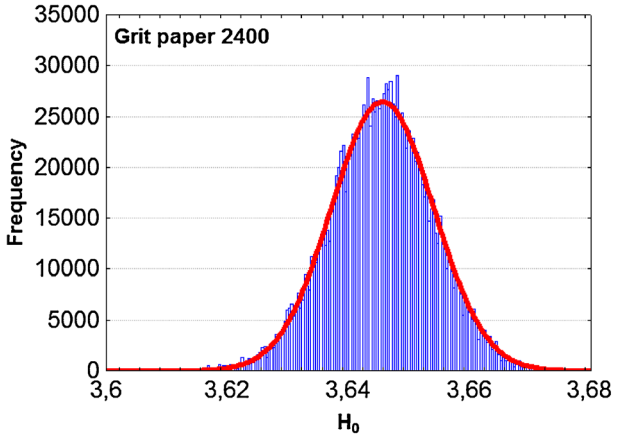


Fig 9. Statistical distribution of macro-hardness $H_0$.

*Multi-scale roughness treatment method*

Surface roughness parameters are very important for surface study (Nowicki, '85). However, the evaluation length value of the profile has a crucial effect on the roughness parameter (Scott *et al*., 2005; Jordan and Brown, 2006; Narayan *et al*., 2006; Bigerelle *et al*., 2007a, 2012), and different evaluation lengths will give different roughness parameters. The initial roughness profiles are experimentally measured for a given length. However, this length is not suitable for studying the indentation imprint. A relevant evaluation length for the roughness calculation should be selected. Note that this choice is closely related to the size of the indentation imprint. To avoid any intuitive selection, a statistical method to choose the evaluation length is developed. This process needs to divide each experimental profile into equal parts, considered each as an evaluation length. Then, a three-degree polynomial and the least square adjustment method are used to rectify each part of the profile. It permits the removal of the variations that are higher than the evaluation length. Then the roughness parameters for the newly processed profile are computed. A complete description of these

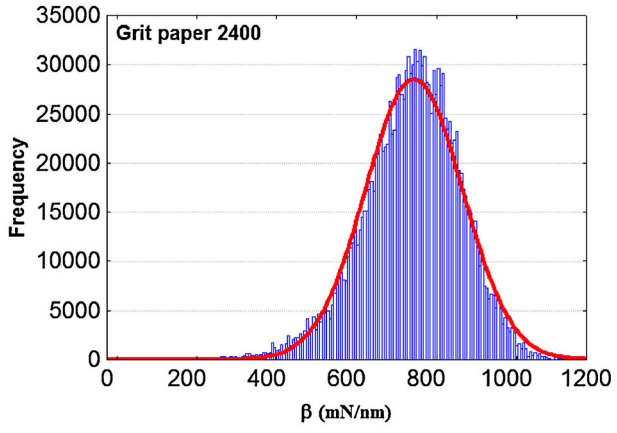


Fig 10. Statistical distribution of indentation size effect coefficient $\beta$.

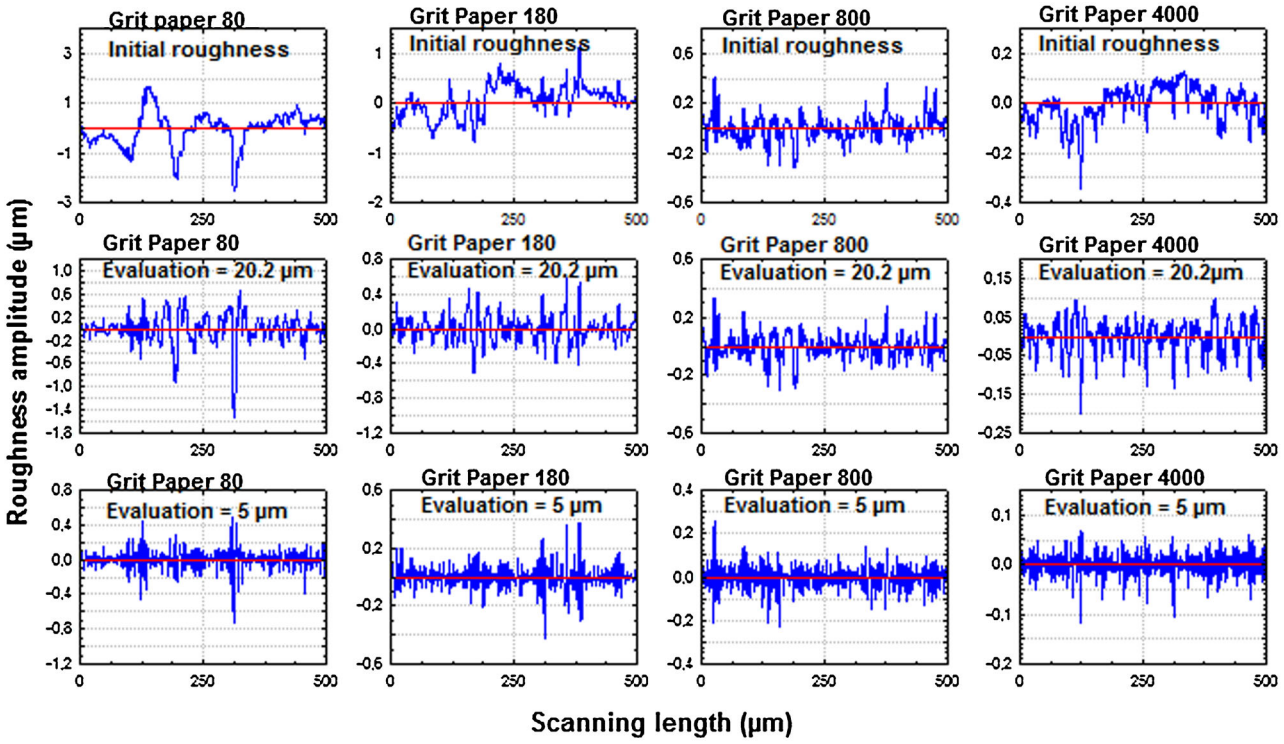


Fig 11. Multi-scale profile reconstructions corresponding to different evaluation lengths.

treatments is given in literature (Bigerelle and Anselme, 2005; Bigerelle *et al*., 2009, 2012).

Figure 11 shows 2D profile roughness using two different evaluation lengths (20.2 and 5 µm) for samples 80, 180, 800, and 4,000. The effect of the evaluation scale on the estimation of the roughness parameters is clearly highlighted. From these filtered profiles, the roughness parameter $R_q$ is estimated. As shown in Figure 12, the root mean square parameter $R_q$ increases logarithmically with the evaluation length for the different samples. However, for a given grit paper (i.e. abrasive grain size) when a critical length is reached, the $R_q$ begins to increase slightly. Note that larger grit paper numbers (i.e. lower abrasive grain size) correspond to lower $R_q$ for all the evaluation length scales. However, it can be observed that the samples can be divided in three main groups: samples belonging to (80–320), or (500–1,200), or (2,400–4,000) grit papers. This aspect will be discussed in the following section.

## Results and Discussions

### Hardness Results and Deviations

Figure 13 depicts the calculated macro-hardness $H_0$ for eleven TiAl6V4 samples. The average macro-hardness varies with the different grit papers (within the range of 3.5–4.1 GPa). From sample 80 to 320, the average value of $H_0$ decreases with the increase of the grit paper (i.e. the decrease of the size of the abrasive grain). This effect might be partly assigned to the influence of the contact surface in the indentation test. For the rougher surface (i.e. polished by the lowest grit paper), the contact surface is small, hence the hardness is high. Within the second and the third group (i.e. grit papers from 500 to 1,200 and from 2,400 to 4,000, respectively), the average value of $H_0$ significantly increases with the increase of paper grit. This effect may be related to the work-hardening phenomenon arising from the polishing process. Such hardening occurs most notably for ductile materials such as the titanium alloy of

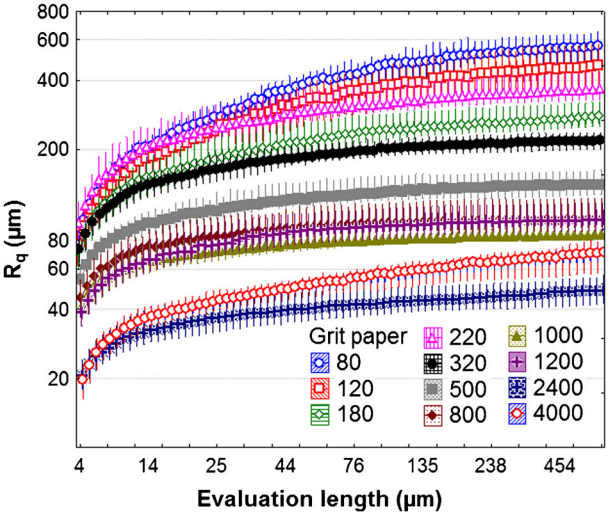


Fig 12. Evolution of the root mean square roughness $R_q$ versus the evaluation length.

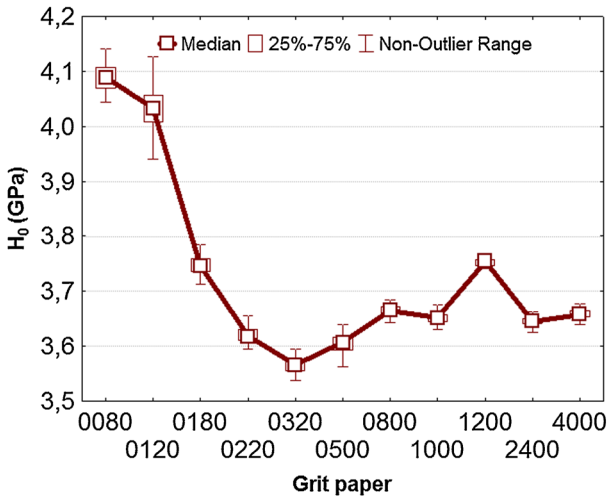


Fig 13. Histogram of the hardness ($H_0$) versus different polishing grit paper.

the present work. Note that these three groups also correspond to the groups indicated in Figure 8. The standard deviations for all the samples are relatively low, down to 0.01 GPa. In comparison with the macro-hardness given by the Nanoindentation MTS$^{TM}$ system (Peseux, Switzerland) using an average value (around 4.3 GPa with the standard deviation is 0.5 GPa), the proposed method gives more accurate quantification of the macro-hardness.

Figure 14 represents the ISE factor values that were calculated using the proposed model. The average values for $\beta$ lie between 310 and 1,600 mN/nm. This figure shows that the ISE does not depend on the sand paper grits. However, the deviation decreases with the increase of the paper grits. As the ISE is closely related to the materials, it appears quite logical that the indentation size effect is not constant. The ISE factor $\beta$ is always greater than zero in the 1,000 Bootstrap protocol. This clearly means that the ISE takes place in this titanium alloy. The literature on the nanoindentation

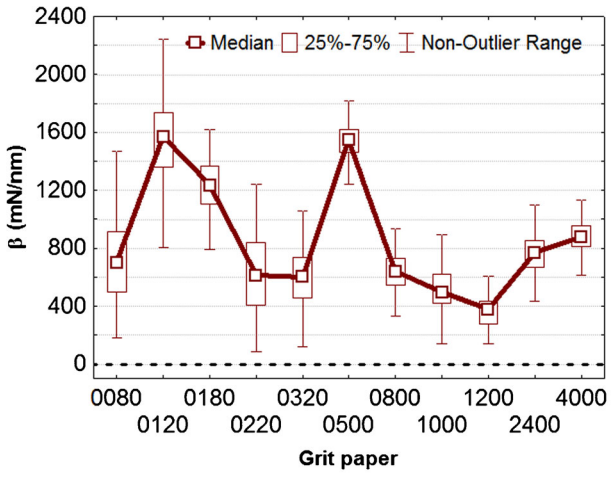


Fig 14. Histogram of the indentation size effect coefficient ($\beta$) versus different polishing grit paper.

test points out that the reasons behind the ISE are multiple, including the pile-up effect. The latter may have a major impact for a very shallow depth (less than about 100 nm) (Iost and Bigot, '96; Kim *et al*., 2007; Lee *et al*., 2008). The occurrence of the pile-up yields an underestimation of the contact depth and the contact area, hence an overestimation of the hardness. In the present work, the topography of the indentation imprint with pile-up is observed with a scanning electron microscope (SEM). An example is given in Figure 15 for samples polished with grit paper 2,400 and 80.

As mentioned above, to estimate the effect of pile-up on hardness in the nanoindentation test, an optical interferometer is used to measure the indentation imprints. Basing on the optical measurement, the pile-up volume is computed by adding the three pile-up volumes measured on each side of the triangle formed by the indent:

$$V_{\text{pileup}} = V_{\text{pileup1}} + V_{\text{pileup2}} + V_{\text{pileup3}}. \tag{8}$$

For each sample, ten nanoindentation tests were used.

A modified macro-hardness $H_{0-\text{cor}}$ is calculated using Equation (9):

$$H_{0-\text{cor}} = \frac{H_0}{1 + \nu_{\text{ratio}}}, \tag{9}$$

where $H_0$ is the macro-hardness calculated by the proposed model (Fig. 13), and $\nu_{\text{ratio}}$ is the ratio of the pile-up volume over the indentation volume:

$$\nu_{\text{ratio}} = \frac{V_{\text{pileup}}}{V_{\text{indent}}}. \tag{10}$$

Figure 16 shows the relationship between the indentation volume, the pile-up volume, the value of $\nu_{\text{ratio}}$, and the modified hardness versus different polishing grit papers. Further on, a statistical analysis of variance, based on the *P*-value calculation (Scherv-ish, '96), was performed to test the significance of the above results, i.e. to test whether the mean calculations of these quantities for different grit papers are similar. Usually, the quantity is considered as significant when its *P*-value is lower than 0.05. As shown in Table 1, the indentation volume, the pile-up volume, and the value of $\nu_{\text{ratio}}$ have very small *P* values, which indicate that these quantities possess different means for different grit papers (i.e. surface amplitude). At the same time, the *P*-value corresponding to the modified macro-hardness is greater than 0.05, which is understandable as the quantity is statistically the same. This observation from a statistical point of view proves that the modified macro-hardness is independent of the grit papers and becomes a constant by taking account of the pile-up during indentation.

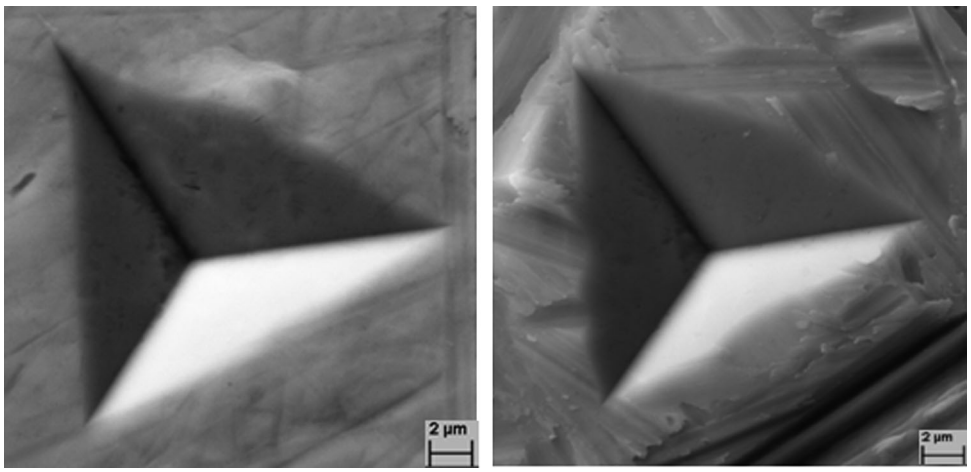


Fig 15. Observation of the nanoindentation prints of TiAl6V4 specimens polished by grit paper 2,400 (left) and 80 (right) using scanning electron microscopy.

The macro-hardness has also been calculated using a classical method:

$$H_{\text{classic}} = \frac{F_{\max}}{A}, \tag{11}$$

where $A$ is the projected contact area, and $F_{\max}$ is the peak load. The projected contact area is estimated from the optical interferometer measurement. For each sample, ten indentation contact areas have been measured. Additionally, an average of the peak loads obtained from the hundred indentation tests on the same

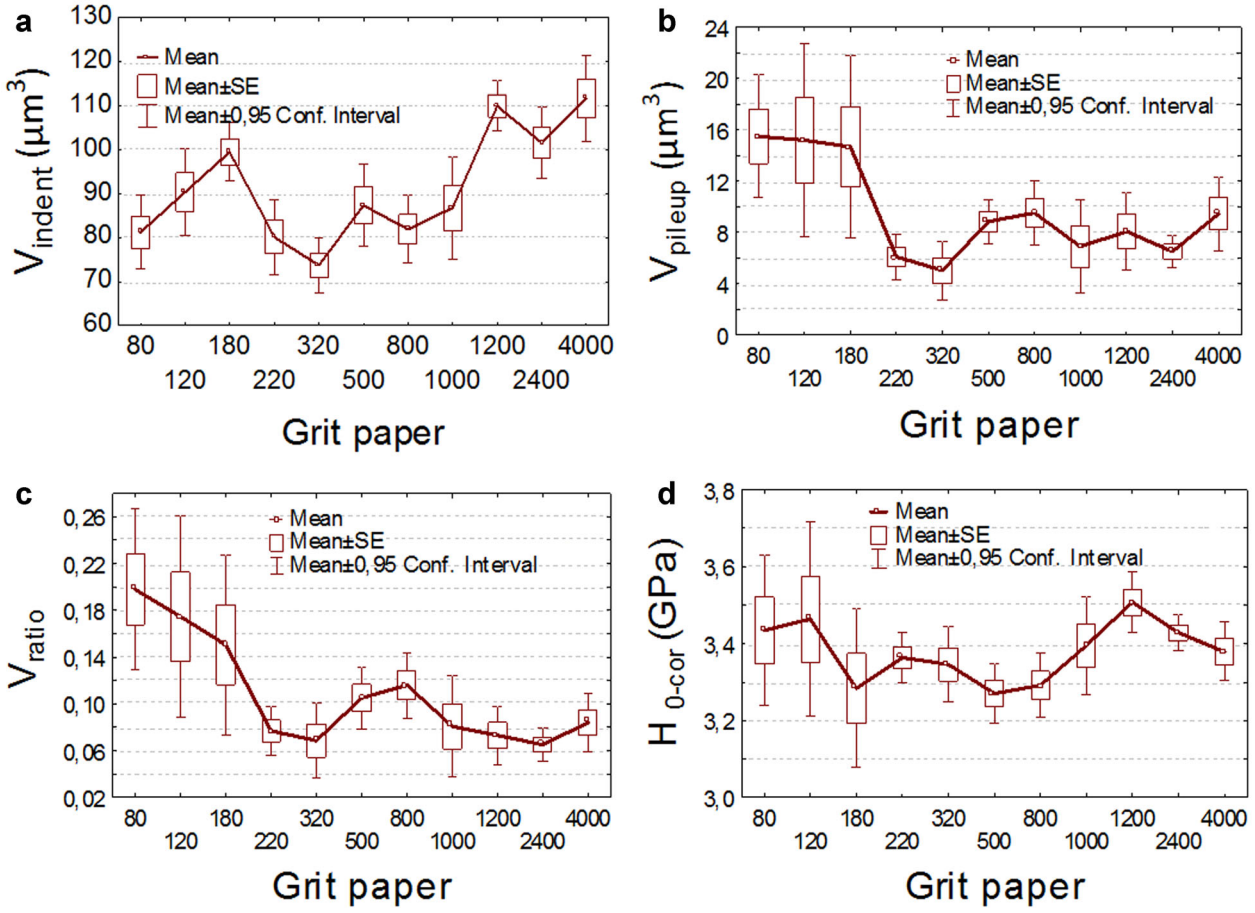


Fig 16. Histogram of (**a**) the indentation volume $V_{\text{indent}}$, (**b**) pile-up volume $V_{\text{pileup}}$, (**c**) $v_{\text{ratio}}$, and (**d**) modified hardness $H_{0\text{–cor}}$ versus different polishing grit paper.

TABLE 1 Analysis of variance for the indentation volume ($V_{indent}$), the pile up volume ($V_{pileup}$), the value of $v_{ratio}$, and the modified hardness ($H_{0-cor}$)

| Variance object | $V_{indent}$ | $V_{pileup}$ | $V_{ratio}$ | $H_{0-cor}$ |
|---|---|---|---|---|
| *F*-value | 11.22539 | 4.55765 | 4.86325 | 1.64282 |
| *P*-value | 0.000000 | 0.00003 | 0.00001 | 0.10569 |

sample is calculated. Therefore, using the "classical" method, ten macro-hardness values are calculated. The results are given in Figure 17. The computed macro-hardness using the classical method is higher than the value obtained by the proposed model. The difference may be explained by the presence of the pile-up, which affects the estimation of the real area of contact. Indeed, the projected area of contact is smaller when compared to the real area of contact, leading to an overestimation of the macro-hardness value calculated by the classical method (Iost and Bigot, '96).

### Stiffness and Young's Modulus

A study of the contact stiffness is required in order to get the elastic properties of the material. In the nanoindentation test, the contact stiffness is calculated from the unloading slope of the load–displacement curve, using well-established models (Li and Bhushan, 2002). This value generally includes a contribution from both the material being tested and the response of the test device itself. The contact stiffness can be used to calculate the reduced Young's modulus $E_r$ using the relation bellow (under the assumption that the behavior remains elastic):

$$E_r = \frac{\sqrt{\pi}}{2}\frac{S}{\sqrt{A}}, \tag{12}$$

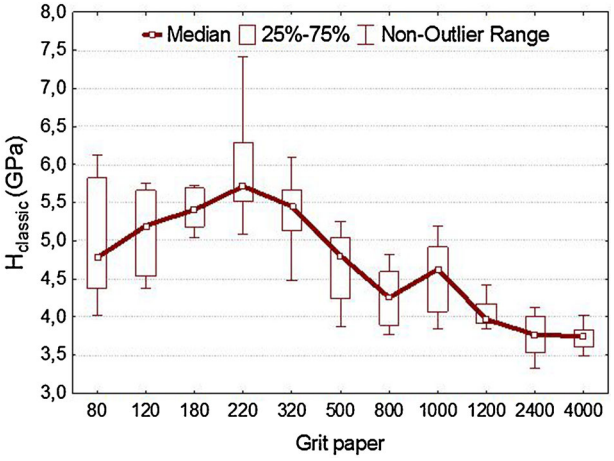


Fig 17. Macro-hardness calculated using classical method versus different polishing grit paper.

where $S$ is the stiffness of contact, and $A$ is the contact area. In the case of the Berkovich indenter, $A$ is given by:

$$A = 24.56h_c^2. \tag{13}$$

The reduced Young's modulus $E_r$ is a function of the indenter's and the specimen's elastic modulus. It is given by:

$$\frac{1}{E_r} = \frac{1-\nu^2}{E} + \frac{1-\nu_i^2}{E_i}, \tag{14}$$

where $E$ and $\nu$ are the elastic modulus and the Poisson's ratio for the tested material, respectively. $E_i$ and $\nu_i$ are the elastic modulus and the Poisson's ratio for the indenter. In the case of a diamond indenter, the following elastic constants $E_i = 1{,}143$ GPa and $\nu_i = 0.07$ are used (Klein and Cardinale, '93).

A relationship between the contact stiffness and the contact depth for an isotropic material can be obtained by substituting Equation (13) into Equation (12):

$$S = \frac{2\sqrt{24.56}h_c}{\sqrt{\pi}}E_r. \tag{15}$$

Equation (15) indicates that the contact stiffness is linearly proportional to the indentation depth.

The contact stiffness evolution with the indentation depth is shown in Figure 18 for the 11 samples. For comparison, the contact stiffness using the CSM method is also indicated. Linear relationships are clearly observed for the different grit papers. Using a least square method, the corresponding slopes are estimated. As indicated in Figure 19, the different slopes are nearly equal. Hence, the stiffness of the contact seems to be not affected by the surface roughness or the surface hardening due to the mechanical polishing.

The Young's modulus of the different samples is computed using Equations (14) and (15):

$$E = \frac{1-\nu^2}{(1/E_r) - ((1-\nu_i^2)/E_i)} = \frac{1-\nu^2}{((2\sqrt{24.56}h_c)/S\sqrt{\pi}) - ((1-\nu_i^2)/E_i)}, \tag{16}$$

where $\nu = 0.3$ for titanium alloy.

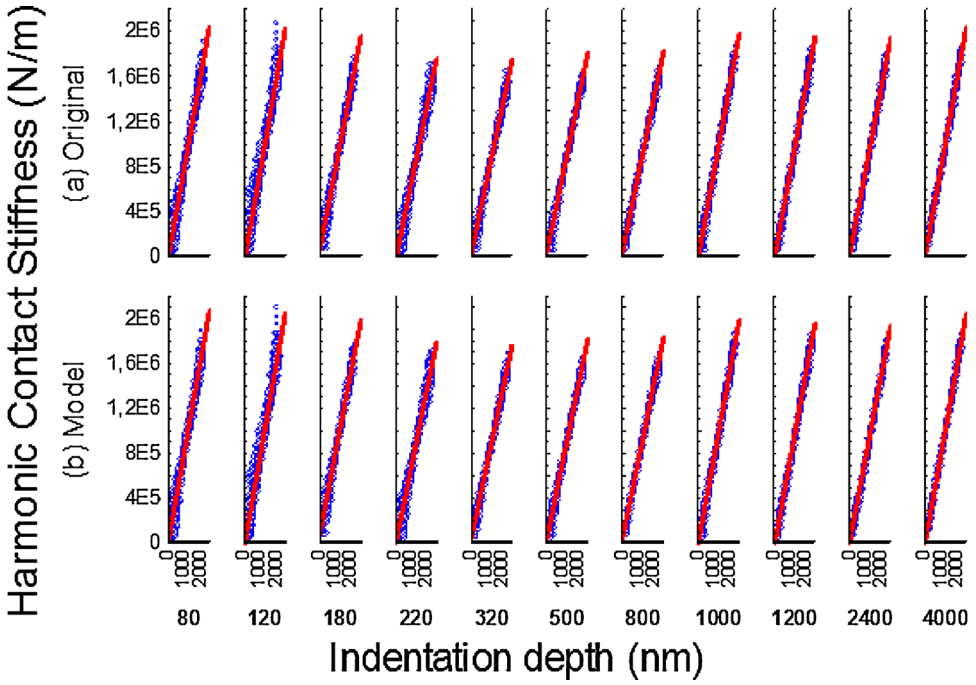


Fig 18. Harmonic contact stiffness of the 11 samples obtained by (**a**) the CSM and (**b**) the proposed model.

Figure 20 represents the evolution of (a) the original Young's modulus and (b) the calculated Young's modulus, which takes into account the first contact error in the proposed model. When the shifting model is applied, the numerical Young's modulus is more gather than the original one. The shifting decreases the dispersion in the Young's modulus calculation. However, for small indentation depths (less than 100 nm), a poor evaluation of the Young's modulus is observed, which can be related to the first contact detection error. The latter is more critical for small depth values (see $h_c$ in Eq. 16). Note that for higher indentation depth (>100 nm), as expected, the calculated Young's modulus remains almost constant for the 11 tested samples. The estimated value is around 136 ± 20 GPa (see Fig. 21), which is consistent with data from the literature for this material (i.e. 105–120 GPa).

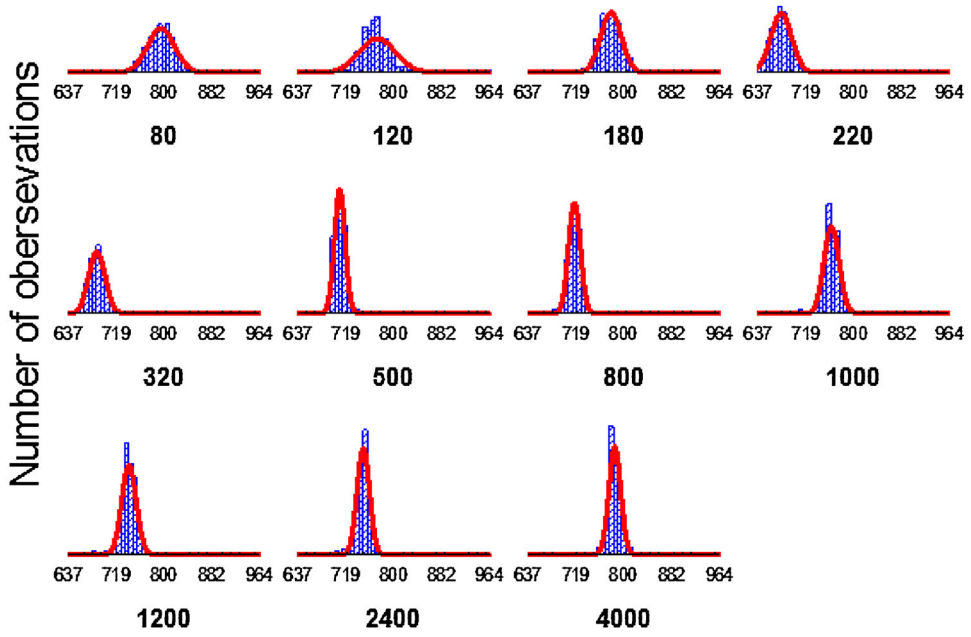


Fig 19. Slope of Stiffness (N/m) versus indentation depth (nm).

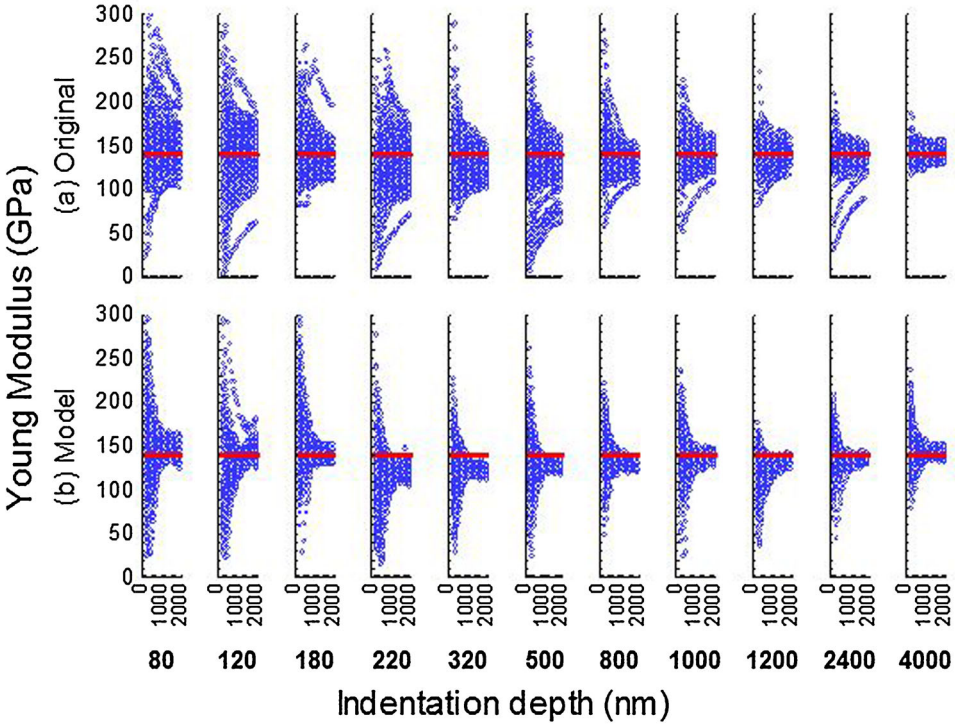


Fig 20. Evolution of (**a**) the experimental Young's modulus and (**b**) the calculated Young's modulus with the contact depth.

**Relation Between Zero Position and Roughness**

Figure 22 shows the distribution calculated for the deviation ($\Delta h_c$) between the experimental loading curve and the simulated one using Bernhardt's law. It is worth noting that data scattering decreases for a high grit paper (i.e. a smooth surface). This scatter is characterized by the standard deviation, which increases from 49.51 to 146.98 nm for the specimen polished with grit paper 4,000 and 80, respectively. Hence, roughness seriously affects the first contact detection.

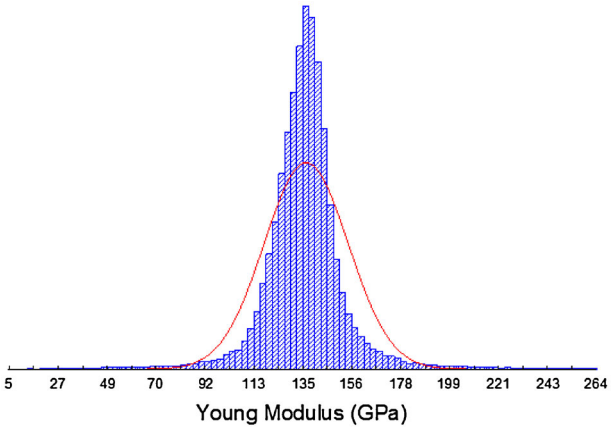


Fig 21. Histograms of the Young's modulus of the TA6V4 computed from Equation (15).

Nevertheless, an appropriate selection of roughness parameters is far from being simple because of the effect of the evaluation length. The difficulty lies in choosing the scale at which the measured roughness influences the first contact detection value. To solve this problem, a multi-scale analysis of the roughness is applied to find the most accurate scale for the evaluation of each roughness parameter. The basic idea is that the best scale for roughness identification is given when the optimal linear relation is found between the standard deviation of the zero position $\sigma(\Delta h_c)$ and the RMS roughness values $R_q$, calculated using the selected evaluation length. The results suggest that the best evaluation value for roughness characterization is around 20 μm, which corresponds to the highest point when the coefficient $R^2$ is close to 1 in Figure 23 and to the lowest point in Figure 24.

A more realistic representation of the profile form is given without including artificial roughness (shown in Fig. 11). Figure 25 shows that there is a linear relation between the standard deviation of the zero position and the RMS value of roughness, when calculated using an evaluation length of 20 μm. The latter is in the same order of indenter (15 μm). It clearly means that the linear relation between roughness and the zero position is due to a roughness below the indenter size, since all wave form higher than this size is removed by the high-pass filter process. It shows the effectiveness of the zero-point correction. The proposed model allows estimation of the mechanical properties, based on the

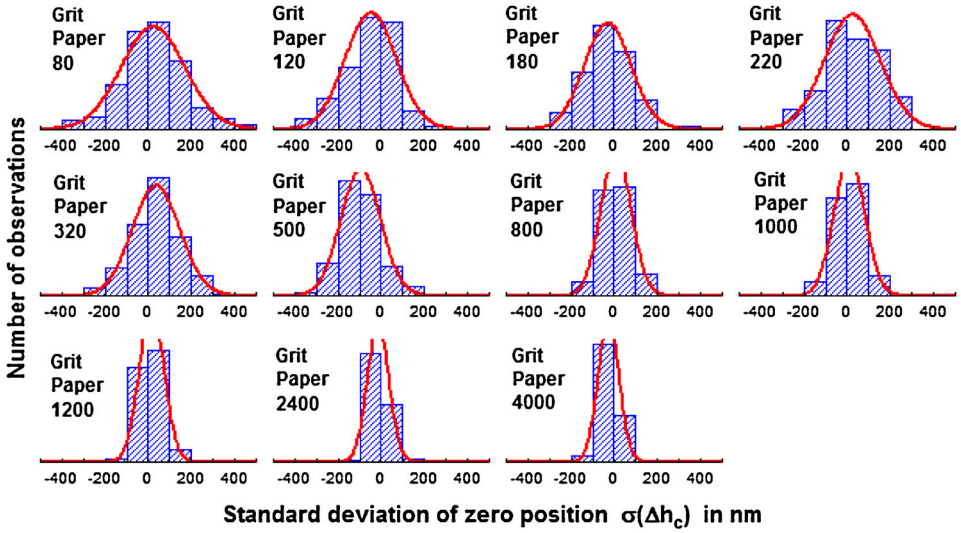


Fig 22. Distribution of zero position for 11 samples.

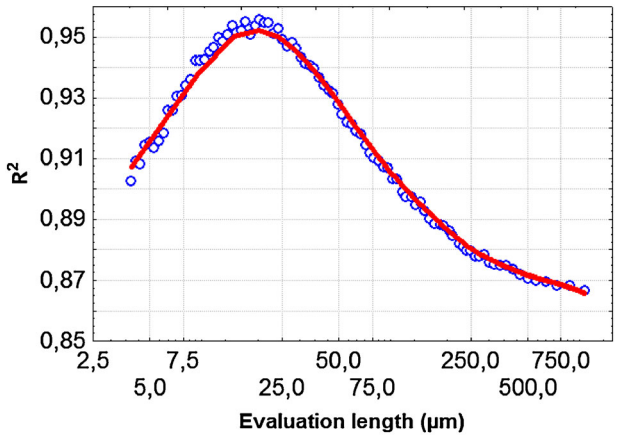


Fig 23. Evolution of the linear correlation coefficient for the relation between the standard deviation $\sigma(\Delta h_c)$ and roughness $R_q$ calculated using different evaluation length.

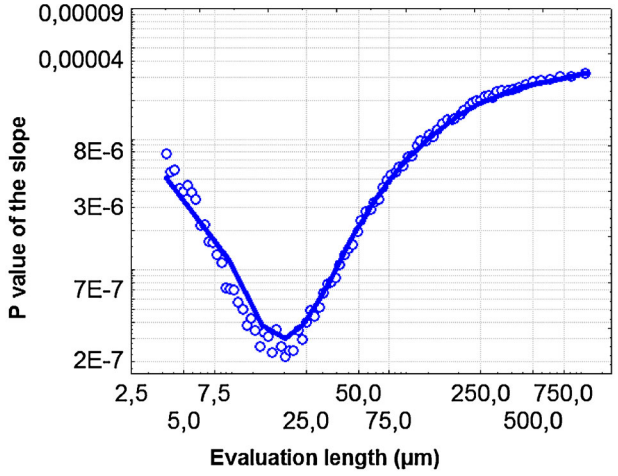


Fig 24. Evolution of the slope of the regression line between the standard deviation $\sigma(\Delta h_c)$ and roughness $R_q$ calculated using different evaluation length.

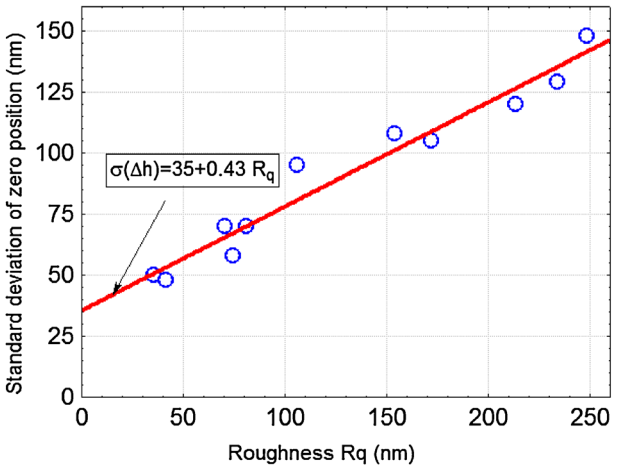


Fig 25. Relation between the standard deviation of zero position and roughness $R_q$.

nanoindentation test on a rough surface, without bias linked to the roughness itself.

## Conclusions

This paper describes a new model for determining the macro-hardness and indentation size effect, based on the load–indentation depth curve in nanoindentation test. The approach is based upon the least squared method regression analysis, treating several experimental curves as a whole. The locations of all the nanoindentation loading curves are set by a specifically first contact error ($\Delta h_c$), defined as the gap between the experimental loading curve and the simulated one using the Bernhardt's law. Thanks to this novel model, nano-indentation tests performed on eleven TiAl6V4

specimens with different surface roughness are analyzed. The estimated macro-hardness using the proposed approach are in the range of 3.5–4.1 GPa, with a small deviation around 0.01 GPa, which is more accurate than the one given by the Nanoindentation MTS$^{TM}$ system, which uses an average value (around $4.3 \pm 0.5$ GPa). Almost similar values are obtained after considering the correction of the real area of contact using the volume pile-up. Moreover, a multi-scale analysis is performed to determine the evaluation length, which leads to an appropriate description of the surface topography. A linear relation between the standard deviation of the zero position $\sigma(\Delta h_c)$ and the standard deviation of the roughness $R_q$ is found. This result shows the influence of surface roughness on the nanoindentation tests. It is found that the best evaluation length is in the order of 20 μm, which is similar to the indenter (15 μm). Therefore, the zero-point correction is effective for estimating mechanical properties, using the nanoindentation test on a rough surface without bias linked to the roughness itself.

## References


Aguilar-Santillan J. 2008. Elastic and hardness anisotropy and the indentation size effect of pyrite (FeS2) single crystal. Acta Mater 56:2476–2487.

Bernhardt E. 1941. On microhardness of solids at the limit of Kick's similarity law. Z Metallkd 33:135–144.

Bigerelle M, Anselme K. 2005. Bootstrap analysis of the relation between initial adhesive events and long-term cellular functions of human osteoblasts cultured on biocompatible metallic substrates. Acta Biomater 1:499–510.

Bigerelle M, Iost A. 1999. Bootstrap analysis of FCGR, application to the Paris relationship and to lifetime prediction. Int J Fatigue 21:299–307.

Bigerelle M, Anselme K, Dufresne E, Hardouin P, Iost A. 2002. An unscaled parameter to measure the order of surfaces: a new surface elaboration to increase cells adhesion. Biomol Eng 19:79–83.

Bigerelle M, Najjar D, Iost A. 2005. Multiscale functional analysis of wear: a fractal model of the grinding process. Wear 258:232–239.

Bigerelle M, Gautier A, Iost A. 2007a. Roughness characteristic length scales of micro-machined surfaces: a multi-scale modelling. Sens. Actuator B-Chem 126:126–137.

Bigerelle M, Mazeran PE, Rachik M. 2007b. The first indenter-sample contact and the indentation size effect in nano-hardness measurement. Mater Sci Eng C 27:1448–1451.

Bigerelle M, Hagege B, El Mansori M. 2008. Mechanical modelling of micro-scale abrasion in superfinish belt grinding. Tribol Int 41:992–1001.

Bigerelle M, Gautier A, Hagege B, Favergeon J, Bounichane B. 2009. Roughness characteristic length scales of belt finished surface. J Mater Process Technol 209:6103–6116.

Bigerelle M, Mathia T, Bouvier S. 2012. The multi-scale roughness analyses and modeling of abrasion with the grit size effect on ground surfaces. Wear 286–287:124–135.

Fischer-Cripps AC. 2000. A review of analysis methods for sub-micron indentation testing. Vacuum 58:569–585.

Fischer-Cripps AC. 2006. Critical review of analysis and interpretation of nanoindentation test data. Surf Coat Tech 200:4153–4165.

Gao HJ, Huang YG. 2003. Geometrically necessary dislocation and size-dependent plasticity. Scripta Mater 48:113–118.

Grau P, Berg G, Fraenzel W, Meinhard H. 1994. Recording hardness testing. Problems of measurement at small indentation depths. Phys Status Solidi A 146:537–548.

Huang YJ, Shen J, Sun Y, Sun JF. 2010. Indentation size effect of hardness of metallic glasses. Mater Des 31:1563–1566.

Iost A, Bigot R. 1996. Indentation size effect: reality or artefact? J Mater Sci 31:3573–3577.

Isselin J, Iost A, Golek J, Najjar D, Bigerelle M. 2006. Assessment of the constitutive law by inverse methodology: small punch test and hardness. J Nucl Mater 352:97–106.

Jang J, Yoo BG, Kim YJ, Oh JH, Choi IC, Bei H. 2011. Indentation size effect in bulk metallic glass. Scripta Mater 64:753–756.

Jordan SE, Brown CA. 2006. Comparing texture characterization parameters on their ability to differentiate ground polyethylene ski bases. Wear 261:398–409.

Kalidindi SR, Pathak S. 2008. Determination of the effective zero-point and the extraction of spherical nanoindentation stress–strain curves. Acta Mater 56:3523–3532.

Kick F. 1885. Das Gesetz der proportionalen Widerstände und seine Anwendungen: Felix.

Kim J, Kang S, Lee J, Jang J, Lee Y, Kwon D. 2007. Influence of surface-roughness on indentation size effect. Acta Mater 55:3555–3562.

Kim J, Lee B, Read D, Kwon D. 2005. Influence of tip bluntness on the size-dependent nanoindentation hardness. Scripta Mater 52:353–358.

Klein CA, Cardinale GF. 1993. Young's modulus and Poisson's ratio of CVD diamond. Diamond Relat Mater 2:918–923.

Lee Y, Hahn J, Nahm S, Jang J, Kwon D. 2008. Investigations on indentation size effects using a pile-up corrected hardness. J Phys D Appl Phys 41:074027.

Li XD, Bhushan B. 2002. A review of nanoindentation continuous stiffness measurement technique and its applications. Mater Charact 48:11–36.

Liu Y, Ngan AHW. 2001. Depth dependence of hardness in copper single crystals measured by nanoindentation. Scripta Mater 44:237–241.

Marteau J, Maxence B, Xia Y, Mazeran PE, Bouvier S. 2013. Quantification of first contact detection errors on hardness and indentation size effect measurements. Tribol Int 59:154–162.

Mukhopadhyay N, Paufler P. 2006. Micro-and nanoindentation techniques for mechanical characterisation of materials. Int Mater Rev 51:209–245.

Najjar D, Bigerelle M, Iost A. 2003. The computer-based bootstrap method as a tool to select a relevant surface roughness parameter. Wear 254:450–460.

Narayan P, Hancock BC, Hamel R, Bergstrom TS, Childs BE, Brown CA. 2006. Differentiation of the surface topographies of pharmaceutical excipient compacts. Mater Sci Eng A 430:79–89.

Nix WD, Gao HJ. 1998. Indentation size effects in crystalline materials: a law for strain gradient plasticity. J Mech Phys Solids 46:411–425.

Nowicki B. 1985. Multiparameter representation of surface roughness. Wear 102:161–176.

Ohmori H, Katahira K, Uehara Y, Watanabe Y, Lin W. 2003. Improvement of mechanical strength of micro tools by controlling surface characteristics. Cirp Ann-Manuf Technol 52:467–470.

Oliver WC, Pharr GM. 1992. Improved technique for determining hardness and elastic modulus using load and displacement sensing indentation experiments. J Mater Res 7:1564–1583.

Oliver WC, Pharr GM. 2010. Nanoindentation in materials research: past, present, and future. MRS Bull 35:897–907.

Qu S, Huang Y, Nix WD, Jiang H, Zhang F, Hwan KC. 2004. Indenter tip radius effect on the Nix–Gao relation in micro- and nanoindentation hardness experiments. J Mater Res 19:3423–3434.

Schervish M. 1996. P values: what they are and what they are not. Am Stat 50:203.

Scott RS, Ungar PS, Bergstrom TS, *et al*. 2005. Dental microwear texture analysis shows within-species diet variability in fossil hominins. Nature 436:693–695.

Ullner C. 2000. Requirement of a robust method for the precise determination of the contact point in the depth sensing hardness test. Measurement 27:43–51.

Wei PJ, Tsai PW, Lin JF. 2008. Micro-contact analysis for the initial contact in nanoindentation tests. Tribol Int 41:1247–1254.

Zhang TY, Xu WH, Zhao MH. 2004. The role of plastic deformation of rough surfaces in the size-dependent hardness. Acta Mater 52:57–68.

Zhanga TY, Xu WH. 2002. Surface effects on nanoindentation. J Mater Res 17:1716.